Coherent phonon detection gated by transient spin-polarized electrons

C. Li and R. T. Harley

Department of Physics and Astronomy, University of Southampton, Southampton SO17 1BJ, United Kingdom

P. G. Lagoudakis

Department of Physics and Astronomy, University of Southampton, Southampton SO17 1BJ, United Kingdom
and Skolkovo Institute of Science and Technology, Moscow, Russian Federation

O. B. Wright and O. Matsuda*

Division of Applied Physics, Faculty of Engineering, Hokkaido University, Sapporo 060-8628, Japan

Manipulating electron spins on ultrashort timescales shows promise in the field of data processing. Because of the direct electron-photon coupling, photons have been widely used for such studies, but not phonons. Here we tie coherent phonon detection to transient spin populations. We optically excite gigahertz picosecond phonon wave packets in a metal-coated GaAs slab containing $GaAs/Al_{0.4}Ga_{0.6}As$ multiple quantum wells on the opposite side. Before the phonon wave-packet arrival, circularly polarized light induces a transient spin polarization. Phonon-induced ultrafast polarization rotation and reflectivity changes contingent on the transient spin population are detected by a heterodyne modulation technique. With an analytical model, we posit the presence of significant second-order interactions, enabled by spins, in the coherent-phonon optical detection. Applications include transient spin population monitoring and novel spintronic nanodevices.

Picosecond coherent phonon wave packets generated and detected in solids by ultrashort laser pulses have led to many developments in fundamental physics and nanomaterial characterizations [1–4]. Coherent phonon detection relies on a variety of physical mechanisms [5]: Acoustic strain can couple via the photoelastic effect [1] to the refractive index, via atomic motions to optical phase and deflection or to x-ray diffraction [6–8], via the deformation potential to the band gap of semiconductors [1,9,10], to the energy levels or photocurrent of quantum wells [11,12], or to polaritons in microcavities [13]. Such detection can also be accomplished using polarized light via strain-induced variations in magnetic anisotropy that effects the spontaneous magnetization (**M**) direction in magnetic semiconductors or ferromagnetic metals [14,15]. This interaction is enabled by **M**, a permanent vector field frozen in by the anisotropy energy (the change in free energy upon rotation of **M**). The field of spintronics is based on the polarization of electron spins in a wider range of materials [16,17] and shows promise in ultrafast switching by photons and mechanisms for nanoscale data processing. However, the effect of *transient* spin populations in such materials, i.e., that decay away to leave **M**=0, on the optical detection of picosecond phonon wave packets has rarely been studied, primarily because such an ultrafast interaction is not known to exist as there is no recognized direct mechanism for coupling phonons to transient spins. However, phonons and spins couple to atomic motion and

to the band structure of the host solid, respectively, both of which couple to changes in the dielectric constant. This provides an indirect route for a phonon-spin interaction because a phonon-induced change in optical properties will induce a second-order change in spin-induced optical activity. By means of a heterodyne technique based on Kerr optical-polarization rotation spectroscopy that is only sensitive to the joint presence of phonons and spins, we harness this phonon-spin interaction to detect picosecond coherent phonon wave packets in the presence of optically excited transient conduction-band spin-polarized electron populations in GaAs/AlGaAs multiple quantum wells (MQWs).

Figure 1(a) shows the sample, which is mounted in a cryostat at 90 K to facilitate coherent phonon propagation (see Supplemental Material [18] and references therein [19–31]). A $GaAs/Al_{0.4}Ga_{0.6}As$ MQW layer was grown on a semi-insulating (110)-oriented GaAs substrate of thickness 106 μm (both sides polished), as follows: the GaAs substrate, a 500-nm GaAs buffer layer, 20 $GaAs/Al_{0.4}Ga_{0.6}As$ QWs each with a 7.5-nm GaAs well, and a 12.5-nm $Al_{0.4}Ga_{0.6}As$ barrier layer, giving a total MQW thickness of 412.5 nm, and finally a 25-nm GaAs capping layer, all with (110) orientation. This sample was previously used to study Kerr rotation at room temperature [32].

The bulk GaAs light- and heavy-hole band degeneracy (total angular momentum quantum number $m_j = \pm 1/2$ and $\pm 3/2$, respectively) at the Γ point is lifted by quantum confinement in GaAs QWs, allowing higher efficiency transient spin-polarization excitation by circularly-polarized light ($\Delta m_j = \pm 1$) [33,34] at a wavelength $\sim$790 nm, i.e., at the
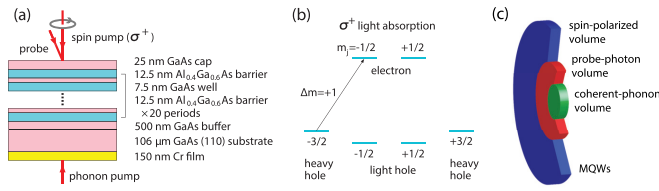
*omatsuda@eng.hokudai.ac.jp

FIG. 1. (a) Sample and beams. (b) Level diagram. (c) Overlapping volumes in MQW layer for spin-polarization, optical probing and coherent-phonon passage (not to scale).
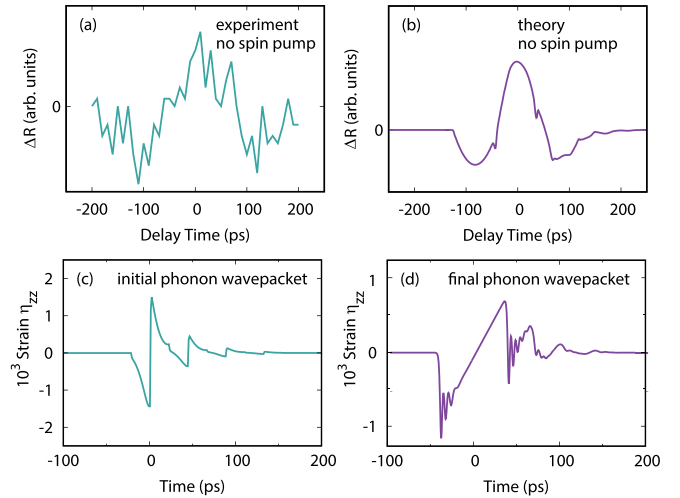

FIG. 2. (a) Phonon-induced transient reflectivity variation ($\Delta R(t)$) with no spin pump, from the two-beam experiment. (b) Theoretical $\Delta R(t)$. (c) Calculated initial longitudinal strain profile $\eta_{zz}(t)$ of the phonon wavepacket transmitted from the Cr film to GaAs. (d) Calculated final strain profile.

hh1-e1 transition at 90 K (see Supplemental Material [18]). This is schematically depicted in Fig. 1(b) for excitation with $\Delta m_j = +1$ light (σ^+). (110)-oriented QWs are favored over (100) owing to their longer spin relaxation time [35]. MQWs further serve to extend the effective volume of the photon-spin interaction. Spin polarization is also produced in the GaAs cap and substrate, but with a lower efficiency [33]. Moreover, the spin lifetime is much shorter ($\tau_{GaAs} < 100$ ps) than that in the MQWs ($\tau_{MQW} > 500$ ps) [35,36], in turn, much less than typical excited electron lifetimes (>10 ns) in both [37]. If probing is done at a time $\gtrsim \tau_{GaAs}$ and $\lesssim \tau_{MQW}$ after spin-pump excitation, spin-polarization measurements will therefore be sensitive to the electrons in the MQWs.

The output of a fs laser (Ti:sapphire regenerative amplifier, wavelength 790 nm, repetition rate 250 kHz, pulse duration $\sim$150 fs) is split into three beams termed the phonon pump, spin pump and probe. The pulse arrival times are varied independently using probe- and phonon-pump delay lines with a $\sim$10-ps step (see Supplemental Material [18]). Picosecond longitudinal phonon wave packets are generated in a 150-nm polycrystalline Cr film on the substrate rear side by the phonon pump ($\sim$0.23 μJ per pulse, spot radius 30 μm at $1/e^2$ intensity) at normal incidence and propagate through the substrate to the MQWs. Oppositely circularly polarized (σ^+ for right and σ^- for left) spin pumps ($\sim$6 nJ per pulse, spot radius 150 μm) at normal incidence excite spin-polarized electrons in the MQW conduction band with an estimated carrier density $N \sim 10^{17}$ cm^{-3} on the sample front side ($\sim$5 $\times$ 10^{11} cm^{-2} per QW layer, with N similar to that used elsewhere on this type of sample [38]) and the cofocused linearly polarized probe ($\sim$0.6 nJ per pulse, spot radius 90 μm) at 3.6° incidence monitors reflectivity R and spin polarization from time-resolved intensity and Kerr rotation, respectively [1,39]. (See Supplemental Material [18] for the optical absorption profile in the MQWs.) A schematic of the interaction volumes is shown in Fig. 1(c). The spot size for the phonon pump is chosen to maximize the phonon intensity, thereby allowing us to exploit elastic nonlinearity to obtain sharp features in the arriving phonon wave packet.

We conduct two types of experiments. In the *two-beam* case, the spin pump is blocked and the phonon pump and probe are chopped at frequencies $f_1 = 1500$ Hz and $f_2 = 1200$ Hz, respectively, with lock-in detection of probe $\Delta R(t)$ as a function of the probe/phonon-pump time delay t at $f_1 + f_2$. This heterodyne technique avoids contamination of the probe light by the phonon pump. In the *three-beam* case, we modulate the phonon and spin pumps at $f_1 = 1500$ Hz and $f_2 = 1200$ Hz, respectively, again with $f_1 + f_2$ detection.

Combining heterodyne and Kerr-rotation detection in this way crucially allows one to selectively access *only* the joint presence of spin populations and acoustic phonons. This assumes that a coupling to the optical modulation of this joint presence exists, something that we aim to demonstrate. The probe/spin-pump delay is set to 70 ps ($\sim \tau_{GaAs}$, $\ll \tau_{MQW}$), whereas that for the probe/phonon-pump is varied. Kerr rotation is measured by dividing the reflected probe light (intensity I) into two cross-polarized components of equal intensity ($I_A = I_B = I/2$) and monitoring $\Delta I_{A-B}(\sigma^\pm) = \Delta I_A(\sigma^\pm) - \Delta I_B(\sigma^\pm)$. For oblique optical probe incidence, $\Delta I_{A-B}(\sigma^\pm)$, in general, contains a non-Kerr contribution owing to the difference in R for s- and p-polarization components. We therefore monitor $[\Delta I_{A-B}(\sigma^+) - \Delta I_{A-B}(\sigma^-)]/(2I)$ to obtain the Kerr rotation $\Delta\theta$, i.e., the angle of rotation of linear polarization owing to the spin polarization. We also confirmed separately that $\Delta I_{A-B}(\sigma^\pm)$ have opposite polarity. In addition, we monitor the variation of the reflected probe intensity $\Delta I(\sigma^\pm) = \Delta I_A(\sigma^\pm) + \Delta I_B(\sigma^\pm)$ and use $[\Delta I(\sigma^+) + \Delta I(\sigma^-)]/(2I)$ to obtain $\Delta R(t)/R$ in the three-beam experiments, although it is spin independent. Typical values for the relative modulations $\Delta R/R$ and $\Delta\theta$ are $\lesssim 10^{-5}$ (The corresponding relative modulations at a point on the probe spot axis are therefore $\lesssim 10^{-4}$.)

The two-beam experiments reveal phonon wave-packet detection by the MQWs; the measured probe reflectivity variation $\Delta R(t)$ is shown in Fig. 2(a) for times ($t = 0$) around the phonon arrival at the front surface. Superimposed on the random measurement noise is a clear bipolar variation in ΔR. To understand this, we model the phonon wave packet and its interaction with the MQWs.

Figure 2(c) shows the initial wave-packet profile from a model based on ultrafast electron diffusion and thermoelastic generation in Cr (see Supplemental Material [18]). A bipolar component of strain amplitude $\sim 10^{-3}$ is followed by components arising from multiple acoustic reflections inside the Cr film [1,3,4]. Figure 2(d) shows the calculated profile on

arrival at the MQWs (see Supplemental Material [18] for the nonlinear-propagation and temperature-rise calculations). An N-shaped leading component and tail is formed at frequencies in the range 10 GHz–0.5 THz [2,40]. Owing to reflection from the surface, this wave packet makes two passes through the MQWs. The acoustic-impedance difference between the MQWs and GaAs is neglected (see Supplemental Material [18]).

The phonon wave packet perturbs the MQW permittivity and interface positions. We first derive $\Delta R(t)$ [41]: For monochromatic probe light (of angular frequency ω) subject to a quasistatic permittivity modulation ($\Delta \boldsymbol{\varepsilon}$), the optical electric field $\mathbf{E}(z)$, where z points directly downward from the surface, is obtained by solving

$$\{\mathbf{L} + k^2[\boldsymbol{\varepsilon}(z) + \Delta \boldsymbol{\varepsilon}(z)]\}\mathbf{E}(z) = 0,$$

$$\mathbf{L} \equiv \begin{pmatrix} d^2/dz^2 & 0 & 0 \\ 0 & d^2/dz^2 & 0 \\ 0 & 0 & 0 \end{pmatrix}, \qquad (1)$$

where k is the optical wave number ($k = \omega/c$, c the vacuum light speed) and $\boldsymbol{\varepsilon}(z)$ is the unperturbed permittivity tensor. We assume lateral homogeneity and normal plane-wave incidence (a good approximation here). For a small perturbation, one makes use of the solution $\mathbf{E}_0(z)$ of the nonperturbed sys-

tem: $[\mathbf{L} + k^2\boldsymbol{\varepsilon}(z)]\mathbf{E}_0(z) = 0$ and the 3×3 Green's function matrix $\mathbf{G}$, which satisfies $[\mathbf{L} + k^2\boldsymbol{\varepsilon}(z)]\mathbf{G}(z, z') = -\delta(z - z')\mathbf{I}$, where $\mathbf{I}$ is the identity matrix. $\mathbf{E}$ is given by the series [41,42]

$$\mathbf{E}(z) = \mathbf{E}_0(z) + \Delta \mathbf{E}(z)$$

$$\simeq \mathbf{E}_0(z) + k^2 \int_{-\infty}^{\infty} \mathbf{G}(z, z') \Delta \boldsymbol{\varepsilon}(z') \mathbf{E}_0(z') dz'$$

$$+ k^4 \iint_{-\infty}^{\infty} \mathbf{G}(z, z') \Delta \boldsymbol{\varepsilon}(z') \mathbf{G}(z', z'') \Delta \boldsymbol{\varepsilon}(z'') \mathbf{E}_0(z'') dz' dz'' + \cdots .$$

$$(2)$$

The external electric field $\mathbf{E}_0$ is a sum of incident ($\mathbf{E}_{0i}$) and reflected ($\mathbf{E}_{0r}$) waves. The second term on the right of Eq. (2) is the perturbation of $\mathbf{E}$ from single-scattering processes (first order), whereas the third term is from sequential double-scattering processes (second-order). The Green's function is given elsewhere [42,43]. $|\Delta \mathbf{E}|/|\mathbf{E}_0|$ in the second term (first-order perturbation) in Eq. (2) is much larger than that in the third term (of second order), hence the truncation of the expansion of Eq. (2).

For the two-beam experiments, $\Delta \boldsymbol{\varepsilon}(z)$ is divided into a surface-and-interface displacement term $\Delta \boldsymbol{\varepsilon}_{\mathrm{if}}(z)$ and a photoelastic term $\Delta \boldsymbol{\varepsilon}_{\mathrm{pe}}(z)$. The former is given by

$$\Delta \boldsymbol{\varepsilon}_{\mathrm{if}}(z) = \begin{cases} \boldsymbol{\varepsilon}(z_n - 0) - \boldsymbol{\varepsilon}(z_n + 0) & \text{for } u_z(z_n) > 0 \text{ and } z_n < z < z_n + u_z(z_n) \\ \boldsymbol{\varepsilon}(z_n + 0) - \boldsymbol{\varepsilon}(z_n - 0) & \text{for } u_z(z_n) < 0 \text{ and } z_n + u_z(z_n) < z < z_n \\ 0 & \text{otherwise,} \end{cases} \qquad (3)$$

where $u_z(z)$ is the displacement along the z axis and z_n is the equilibrium position of the interface between the nth layer and the $(n + 1)$th layer, $n = 1$ denoting the top layer, and z_0 is the equilibrium surface position. The sample is considered to consist of a GaAs cap layer and a single homogeneous MQW layer on the GaAs substrate, so $n = 2$ is the MQW layer and $n = 3$ the GaAs buffer-layer/substrate combination (i.e., the substrate). The accuracy of these assumptions is analyzed in full in the Supplemental Material [18]. The photoelastic contribution is linked to strain component η_{zz}: $\Delta \boldsymbol{\varepsilon}_{\mathrm{pe}}(z) \propto \eta_{zz}$ (see Supplemental Material [18]). We are sensitive to the phonon-pump f_1 component of the modulation in $\mathbf{E}$ involving the single-scattering term in Eq. (2), with $\Delta \boldsymbol{\varepsilon} = \Delta \boldsymbol{\varepsilon}_{\mathrm{if}} + \Delta \boldsymbol{\varepsilon}_{\mathrm{pe}}$. The relative reflectivity modulation can be calculated from $\Delta \mathbf{E}$ as follows [44]:

$$\frac{\Delta R}{R} = 2\mathrm{Re}\left(\frac{\mathbf{E}_{0r} \cdot \Delta \mathbf{E}}{|\mathbf{E}_{0r}|^2}\right). \qquad (4)$$

The expected $\Delta R(t)$ from interface motions is a pulse-like variation arising from the passage of the phonon wave packet through the cap/MQW, MQW/substrate and air/cap interfaces, whereas that corresponding to the photoelastic contribution is a Brillouin term characterized by a long-lived oscillation in $\Delta R(t)$, expected at $\sim$50 GHz [9]. We are not able to observe the latter contribution at our level of signal to noise and time step (detection bandwidth $\sim$25 GHz) and so it is omitted in all calculations in this paper, as are analogous terms governed by tensors of the same rank arising from the

deformation potential or inverse magnetostriction. Under this assumption, $\Delta R(t)$ can be expressed as a linear combination of the surface and interface displacements (see Supplemental Material [18]).

Figure 2(b) shows the predicted $\Delta R(t)$ obtained by use of Eq. (4). The density, elastic constant c_{33} (referenced to the crystal axes) and permittivity $\varepsilon_{11} = \varepsilon_{22}$ (likewise referenced) are taken from effective medium theory to be 4.96 kg m^{-3}, 146.1 GPa, and $12.2 + 0.2i$ for the MQW layer [45] and 5.36 kg m^{-3}, 145.7 GPa and $13.6 + 0.6i$ for GaAs [46,47]. $u_z(z_n, t)$ are calculated with no cap/MQW ultrasonic attenuation (see Ref. [41] and the Supplemental Material [18]). The overall variation matches the experiment well when accounting for random noise and our detection bandwidth. According to similar studies in QWs [11], such agreement is expected. This establishes the basics of the theoretical approach as applied to the two-beam experiment.

The three-beam experiments are designed to reveal the spin-gated phonon-wave-packet detection by the MQWs: $\Delta R(t)$ and $\Delta \theta(t)$ are shown in Figs. 3(a) and 3(b), both exhibiting bipolar variations. $\Delta R(t)$ is similar to that for the two-beam case but is opposite in sign. The polarity of ΔR and $\Delta \theta$, however, do not have any significant meaning here, since they depend on the choice of the lock-in detection phase; we choose this phase for maximum $|\Delta R|$ and $|\Delta \theta|$, whereas their polarities remain arbitrary quantities.

To understand these variations, we revisit Eq. (2), including the effect of the spin-polarized electrons. The first required
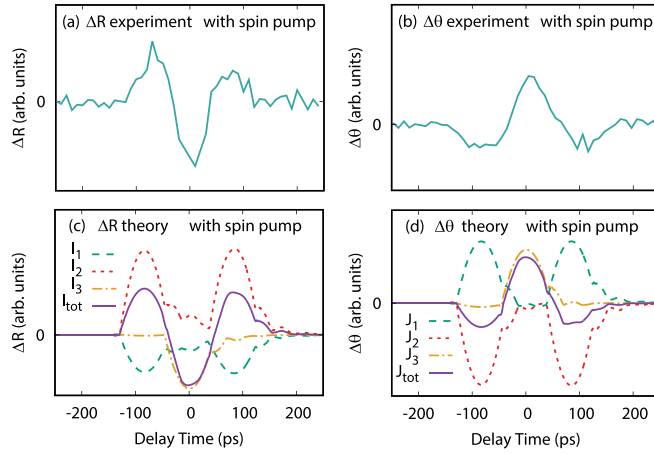
FIG. 3. Results from the three-beam experiment. (a) Phonon-spin-induced reflectivity $[\Delta R(t)]$. (b) Phonon-spin-induced Kerr-rotation $[\Delta\theta(t)]$. (c) Theoretical predictions of the variations in ΔR, I_{tot}, I_1–I_3, and (d) in $\Delta\theta$, J_{tot}, J_1–J_3. Intensity modulation terms I_1, J_1: First-order, by first-order scattering caused by second order in $\Delta\varepsilon$. I_2, J_2: First order, by second-order scattering caused by two first-order scattering processes in $\Delta\varepsilon$. I_3, J_3: Second order, by two first-order scattering processes caused by first-order in $\Delta\varepsilon$.

term comes from the second-order effect in the permittivity modulation $\Delta\varepsilon_{\text{if,el}}$, which is proportional both to $u_z(z_n, t)$ and to the electron densities n^+ and n^- of up and down spins. The total permittivity modulation is given by $\Delta\varepsilon = \Delta\varepsilon_{\text{if}} + \Delta\varepsilon_{\text{el}} + \Delta\varepsilon_{\text{if,el}}$, where $\Delta\varepsilon_{\text{el}}$ is the first-order modulation of ε by the spins. We neglect the second-order effect proportional to both η_{zz} and n, since this would lead to an oscillating term not observed. In accordance with experiments, $\Delta\varepsilon_{\text{if}}$ is modulated at frequency f_1, $\Delta\varepsilon_{\text{el}}$ at f_2, and $\Delta\varepsilon_{\text{if,el}}$ at $f_1 + f_2$.

The explicit form of $\Delta\varepsilon_{\text{el}}$ is given by [48]

$$\Delta\varepsilon_{\text{el}}(z) = \begin{pmatrix} 0 & -ia_e & 0 \\ ia_e & 0 & 0 \\ 0 & 0 & 0 \end{pmatrix} [n^+(z) - n^-(z)]$$
$$+ \begin{pmatrix} b_e & 0 & 0 \\ 0 & b_e & 0 \\ 0 & 0 & b_e \end{pmatrix} [n^+(z) + n^-(z)], \quad (5)$$

where a_e and b_e are layer-dependent constants. The magnetic dipole moment of the spin-polarized electrons is assumed to be z oriented, parallel to the pump incidence. The first term involving a_e—a key term in our detection scheme—is related to the spin polarization $n_+ - n_-$ and Kerr rotation, whereas the second term involving b_e is related to the total spin density $n_+ + n_-$. [The Supplemental Material [18] discusses Eq. (5) and birefringence effects.]

$\Delta\varepsilon_{\text{if,el}}$ is given by Eq. (3) but with $\Delta\varepsilon_{\text{if}}$ replaced by $\Delta\varepsilon_{\text{if,el}}$ on the left-hand side and ε by $\Delta\varepsilon_{\text{el}}$ on the right. We thereby obtain a permittivity modulation by the spins in the parts of the sample protruding or recessed from the equilibrium surface or interface positions.

Using the components $\Delta\varepsilon_{\text{if}}$, $\Delta\varepsilon_{\text{el}}$, and $\Delta\varepsilon_{\text{if,el}}$ of $\Delta\varepsilon$, Eq. (2) yields the electric field modulation

$$\Delta\mathbf{E} = \Delta\mathbf{E}_{\text{if}}^{(1)} + \Delta\mathbf{E}_{\text{el}}^{(1)} + \Delta\mathbf{E}_{\text{if,el}}^{(1)} + \Delta\mathbf{E}_{\text{if,el}}^{(2)}, \quad (6)$$

where the explicit form of each term is given in the Supplemental Material [18]. $\Delta\mathbf{E}_{\text{if}}^{(1)}$, $\Delta\mathbf{E}_{\text{el}}^{(1)}$ and $\Delta\mathbf{E}_{\text{if,el}}^{(1)}$ are first-order scattering terms caused by $\Delta\varepsilon_{\text{if}}$, $\Delta\varepsilon_{\text{el}}$, and $\Delta\varepsilon_{\text{if,el}}$, and possess modulation-frequency components f_1, f_2, and $f_1 + f_2$, respectively. $\Delta\mathbf{E}_{\text{if,el}}^{(2)}$ is a second-order scattering term caused by $\Delta\varepsilon_{\text{if}}$ and $\Delta\varepsilon_{\text{el}}$, and possesses modulation-frequency component $f_1 + f_2$.

$\Delta R/R$ in the three-beam experiment is thus given by

$$1 + \frac{\Delta R}{R} = \frac{|\mathbf{E}_{0r} + \Delta\mathbf{E}|^2}{|\mathbf{E}_{0r}|^2}. \quad (7)$$

$\Delta R(t)$ at frequency $f_1 + f_2$, i.e., associated with the joint phonon-spin presence, is made up of three commensurate intensity-modulations: $\Delta R_{f_1 + f_2} \propto I_{\text{tot}} = I_1 + I_2 + I_3$, where

$$I_1 = 2\text{Re}(\mathbf{E}_{0r} \cdot \Delta\mathbf{E}_{\text{if,el}}^{(1)}),$$
$$I_2 = 2\text{Re}(\mathbf{E}_{0r} \cdot \Delta\mathbf{E}_{\text{if,el}}^{(2)}), \quad (8)$$
$$I_3 = 2\text{Re}(\Delta\mathbf{E}_{\text{if}}^{(1)} \cdot \Delta\mathbf{E}_{\text{el}}^{(1)}).$$

I_1 is the first-order modulation by first-order scattering caused by second-order perturbations in ε, I_2 is the first-order modulation by second-order scattering caused by two successive first-order perturbations in ε, and I_3 is the second-order modulation by two first-order scattering processes caused by first-order perturbations in ε.

Equation (2) indicates that $\mathbf{E}_{0r} \cdot \Delta\mathbf{E}_{\text{if,el}}^{(2)}$ is of the same order as $\Delta\mathbf{E}_{\text{if}}^{(1)} \cdot \Delta\mathbf{E}_{\text{el}}^{(1)}$, implying that $I_2 \sim I_3$. The order estimate for I_1 is somewhat more subtle. Using the equation for $\Delta\varepsilon_{\text{if,el}}$ mentioned above and noting that the finite eigenvalues of $\mathbf{G}$ are of order $1/k$ [42,49], $|\Delta\mathbf{E}_{\text{if,el}}^{(2)}|$ is $\sim \varepsilon_M k_M d_M$ times larger than $|\Delta\mathbf{E}_{\text{if,el}}^{(1)}|$ in the MQW, where ε_M is a relevant permittivity tensor component, k_M the wave number, and d_M the MQW thickness. In our case, $\varepsilon_M k_M d_M \sim 1$, so $I_1 \sim I_2 \sim I_3$.

Measuring $\Delta\theta$ requires taking the intensity difference between two orthogonal polarizations:

$$\Delta\theta \propto |(\mathbf{E}_{0r} + \Delta\mathbf{E}) \cdot \mathbf{e}_1|^2 - |(\mathbf{E}_{0r} + \Delta\mathbf{E}) \cdot \mathbf{e}_2|^2, \quad (9)$$

where $\mathbf{e}_i$ ($i = 1, 2$) are the unit vectors along the two polarization directions, chosen so $|\mathbf{E}_{0r} \cdot \mathbf{e}_1|^2 = |\mathbf{E}_{0r} \cdot \mathbf{e}_2|^2$. The $f_1 + f_2$ component of the Kerr rotation, i.e., that associated with both phonons and spins, is made up of three contributions: $\Delta\theta_{f_1 + f_2} \propto J_{\text{tot}} = J_1 + J_2 + J_3$, where

$$J_1 = 2\text{Re}[(\mathbf{E}_{0r} \cdot \mathbf{e}_1)(\Delta\mathbf{E}_{\text{if,el}}^{(1)} \cdot \mathbf{e}_1)^* - (\mathbf{E}_{0r} \cdot \mathbf{e}_2)(\Delta\mathbf{E}_{\text{if,el}}^{(1)} \cdot \mathbf{e}_2)^*],$$
$$J_2 = 2\text{Re}[(\mathbf{E}_{0r} \cdot \mathbf{e}_1)(\Delta\mathbf{E}_{\text{if,el}}^{(2)} \cdot \mathbf{e}_1)^*$$
$$- (\mathbf{E}_{0r} \cdot \mathbf{e}_2)(\Delta\mathbf{E}_{\text{if,el}}^{(2)} \cdot \mathbf{e}_2)^*], \quad (10)$$
$$J_3 = 2\text{Re}[(\Delta\mathbf{E}_{\text{if}}^{(1)} \cdot \mathbf{e}_1)(\Delta\mathbf{E}_{\text{el}}^{(1)} \cdot \mathbf{e}_1)^*$$
$$- (\Delta\mathbf{E}_{\text{if}}^{(1)} \cdot \mathbf{e}_2)(\Delta\mathbf{E}_{\text{el}}^{(1)} \cdot \mathbf{e}_2)^*].$$

J_1, J_2, and J_3 have a similar origin to I_1, I_2, and I_3. By the same arguments as used for I_1, I_2, I_3, one finds that J_1, J_2, J_3 are of the same order.

The predicted $\Delta R(t)$ and $\Delta\theta(t)$ are shown in Figs. 3(c) and 3(d) together with their contributing components. Following the arguments outlined in the experimental section, we make the simplifying assumption that the spin density in the MQW layer provides the dominant Kerr rotation and ignore the effect

of that in the GaAs cap layer and substrate. The terms a_e and b_e, which, respectively, influence $\Delta\theta$ and ΔR for the MQW layer (a_e and b_e) and for GaAs (b_e only) are adjusted for best fit, giving normalized values $a_e = 1.0 - 0.1i$, $b_e = 0.5 + 0.9i$ for the MQW layer and $b_e = 0.2 + 0.05i$ for GaAs. The accuracy is $\lesssim \pm 5\%$ in all cases. The quantities a_e and b_e are normalized for the MQW layer, i.e., $|a_e| = |b_e| = 1$ to within the experimental error.

In particular, our derived constant a_e for the MQW layer is crucial to the coherent phonon detection in the presence of spin polarization $n_+ - n_-$, without which spin-phonon coupling to $\boldsymbol{\varepsilon}$ could not occur. Only the ratio between the real and imaginary parts of a_e affects the fitted $\Delta\theta(t)$, since the absolute magnitude is arbitrary. [Similarly, only the ratio between b_e for GaAs and the MQWs affects $\Delta R(t)$]. The central portions of $\Delta R(t)$ and $\Delta\theta(t)$ are related to the phonon wave-packet arrival at the sample surface and passage across the cap/MQW interface, whereas the side peaks are related to its passage across the MQW/substrate interface. Good agreement between experiment and theory is again obtained within our experimental bandwidth, validating our theoretical approach and the existence of the spin-phonon coupling to the optical permittivity.

The effect of the transient spin population on the coherent phonon detection is effectively constant in time because of the relatively slow relaxation compared to the phonon wave-packet duration. As in the two-beam predictions, $\Delta R(t)$ and $\Delta\theta(t)$ can thus be expressed as linear combinations of the surface and interface displacements (see Supplemental Material [18]). Although the data of Figs. 2(a) and 3(a) are superficially similar, the data of Fig. 3 are modified by the presence of the spin populations n^+ and n^- and are therefore not identical. (See Supplemental Material [18] for a more detailed discussion of the temporal variations.)

It is important to distinguish our results from similar experiments in ferromagnets [14,15], where the time-resolved strain-induced Kerr modulation results from the rotation of the permanent magnetization vector **M** in an applied magnetic field. This effect, based on inverse magnetostriction, results from the modulation of the magnetization direction by the strain. In contrast, in our experiment the strain-induced Kerr modulation does not arise from a change in the vector direction or magnitude of the spin population by the strain, but rather from the modulation of the optical coupling of the transient spins to the Kerr rotation through phonon-induced ultrafast interface displacements.

In conclusion, we have demonstrated transient-spin gated coherent phonon detection. This paper opens a field of investigation for ultrafast optical modulation in the presence of both coherent phonons and electron spins. Probing how the optical modulation caused by the joint effects of photo-induced spin density and strain depends on material, crystal cut, temperature, phonon polarization, and spin-pump/probe delay should help further quantify the underlying physics, including the absolute determination of the tensorial coupling parameters. Optimizing this phenomenon, for example, by the use of individual high-amplitude acoustic solitons tunable by varying the pump fluence, could lead to new perspectives in phonon-mediated ultrafast spintronic nanodevice applications. In addition, the use of concentrated beams of coherent phonons would allow spatial profiling of the transient spin density on microscopic scales with our technique.

[1] C. Thomsen, H. T. Grahn, H. J. Maris, and J. Tauc, Phys. Rev. B **34**, 4129 (1986).

[2] H. Y. Hao and H. J. Maris, Phys. Rev. B **64**, 064302 (2001).

[3] O. Matsuda, M. C. Larciprete, R. L. Voti, and O. B. Wright, Ultrasonics **56**, 3 (2015).

[4] P. Ruello and V. E. Gusev, Ultrasonics **56**, 21 (2015).

[5] M. Nicoul, U. Shymanovich, A. Tarasevitch, D. von der Linde, and K. Sokolowski-Tinten, Appl. Phys. Lett. **98**, 191902 (2011).

[6] C. Rose-Petruck, R. Jimenez, T. Guo, A. Cavalleri, C. W. Siders, F. Rksi, J. A. Squier, B. C. Walker, K. R. Wilson, and C. P. J. Barty, Nature (London) **398**, 310 (1999).

[7] O. B. Wright and T. Hyoguchi, Opt. Lett. **16**, 1529 (1991).

[8] O. B. Wright and K. Kawashima, Phys. Rev. Lett. **69**, 1668 (1992).

[9] O. B. Wright, B. Perrin, O. Matsuda, and V. E. Gusev, Phys. Rev. B **64**, 081202(R) (2001).

[10] A. V. Akimov, A. V. Scherbakov, D. R. Yakovlev, C. T. Foxon, and M. Bayer, Phys. Rev. Lett. **97**, 037401 (2006).

[11] O. Matsuda, T. Tachizaki, T. Fukui, J. J. Baumberg, and O. B. Wright, Phys. Rev. B **71**, 115330 (2005).

[12] D. Moss, A. V. Akimov, R. P. Campion, M. Henini, C. T. Foxon, L. Eaves, A. J. Kent, and B. A. Glavin, Phys. Rev. B **83**, 245303 (2011).

[13] A. V. Scherbakov, T. Berstermann, A. V. Akimov, D. R. Yakovlev, G. Beaudoin, D. Bajoni, I. Sagnes, J. Bloch, and M. Bayer, Phys. Rev. B **78**, 241302(R) (2008).

[14] A. V. Scherbakov, A. S. Salasyuk, A. V. Akimov, X. Liu, M. Bombeck, C. Brüggemann, D. R. Yakovlev, V. F. Sapega, J. K. Furdyna, and M. Bayer, Phys. Rev. Lett. **105**, 117204 (2010).

[15] J.-W. Kim, M. Vomir, and J.-Y. Bigot, Phys. Rev. Lett. **109**, 166601 (2012).

[16] I. Žutić, J. Fabian, and S. D. Sarma, Rev. Mod. Phys. **76**, 323 (2004).

[17] S. Bader and S. Parkin, Annu. Rev. Condens. Matter Phys. **1**, 71 (2010).

[18] See Supplemental Material at http://link.aps.org/supplemental/10.1103/PhysRevB.103.L241201 for the experimental setup, phonon generation, and nonlinear propagation, light absorption, temperature rise, light scattering, magneto-optic effect, and justification for the three-layer model.

[19] S. Anisimov, B. Kapeliovich, and T. Perelman, Zh. Eksp. Teor. Fiz. **66**, 776 (1974) [Sov. Phys. JETP **39**, 375 (1974)].

[20] T. Saito, O. Matsuda, and O. B. Wright, Phys. Rev. B **67**, 205421 (2003).

[21] *Thermal Conductivity: Metallic Elements and Alloys*, Thermophysical Properties of Matter, edited by Y. S. Touloukian, R. W. Powell, C. Y. Ho, and P. G. Klemens, Vol. 1 (IFI/Plenum, New York, 1970).

[22] *Specific Heat: Metallic Elements and Alloys*, Thermophysical Properties of Matter, edited by Y. S. Touloukian and E. H. Buyco, Vol. 4 (IFI/Plenum, New York, 1970).

[23] *Thermal Expansion: Metallic Elements and Alloys*, Thermophysical Properties of Matter, edited by Y. S. Touloukian and E. H. Buyco, Vol. 12 (IFI/Plenum, New York, 1975).

[24] D. R. Lide, ed., *CRC Handbook of Chemistry and Physics*, 85th ed. (CRC Press, Boca Raton, FL, 2004).

[25] K. H. Schramm, Z. Metallkd. **53**, 729 (1962).

[26] T. A. Driscoll, J. Comput. Phys. **182**, 357 (2002).

[27] W. Chen, H. J. Maris, Z. R. Wasilewski, and S. Tamura, Phil. Mag. B **70**, 687 (1994).

[28] H. Y. Hao and H. J. Maris, Phys. Rev. B **63**, 224301 (2001).

[29] D. J. Dunstan and S. H. B. Bosher, Phys. Stat. Sol. B **235**, 396 (2003).

[30] S. Adachi, *GaAs and Related Materials: Bulk Semiconducting and Superlattice Properties* (World Scientific, Singapore, 1994).

[31] S. Kashiwada, O. Matsuda, J. J. Baumberg, R. L. Voti, and O. B. Wright, J. Appl. Phys. **100**, 073506 (2006).

[32] P. S. Eldridge, P. G. Lagoudakis, M. Henini, and R. T. Harley, Phys. Rev. B **81**, 033302 (2010).

[33] D. T. Pierce and F. Meier, Phys. Rev. B **13**, 5484 (1976).

[34] A. Tackeuchi, S. Muto, T. Inata, and T. Fujii, Appl. Phys. Lett. **56**, 2213 (1990).

[35] Y. Ohno, R. Terauchi, T. Adachi, F. Matsukura, and H. Ohno, Phys. Rev. Lett. **83**, 4196 (1999).

[36] C. P. Weber, C. A. Benko, and S. C. Hiew, J. Appl. Phys. **109**, 106101 (2011).

[37] S. Oertel, J. Hübner, and M. Oestreich, Appl. Phys. Lett. **93**, 132112 (2008).

[38] T. Henn, T. Kiessling, W. Ossau, L. W. Molenkamp, K. Biermann, and P. V. Santos, Rev. Sci. Instrum. **84**, 123903 (2013).

[39] R. T. Harley, O. Z. Karimov, and M. Henini, J. Phys. D: Appl. Phys. **36**, 2198 (2003).

[40] O. L. Muskens, Ph.D. thesis, Universiteit Utrecht (2004).

[41] O. Matsuda and O. B. Wright, J. Opt. Soc. Am. B **19**, 3028 (2002).

[42] O. Matsuda, O. B. Wright, D. H. Hurley, V. Gusev, and K. Shimizu, Phys. Rev. B **77**, 224110 (2008).

[43] T. Saito, O. Matsuda, M. Tomoda, and O. B. Wright, J. Opt. Soc. Am. B **27**, 2632 (2010).

[44] Note, we adopt the definition $\mathbf{A} \cdot \mathbf{B} = A_x^* B_x + A_y^* B_y + A_z^* B_z$ throughout this paper.

[45] B. Djafari Rouhani and J. Sapriel, Phys. Rev. B **34**, 7114 (1986).

[46] S. Adachi, J. Appl. Phys. **58**, R1 (1985).

[47] S. Adachi, *Properties of Aluminum Gallium Arsenide* (INSPEC, London, 1993).

[48] W. Jung, J. Appl. Phys. **36**, 2422 (1965).

[49] O. Matsuda, M. Tomoda, T. Tachizaki, S. Koiwa, A. Ono, K. Aoki, R. P. Beardsley, and O. B. Wright, J. Opt. Soc. Am. B **30**, 1911 (2013).